Structural Variability in Wild-Type and *bchQ bchR* Mutant Chlorosomes of the Green Sulfur Bacterium *Chlorobaculum tepidum*

Swapna Ganapathy,[†,⊥] Gert T. Oostergetel,[‡] Michael Reus,[§] Yusuke Tsukatani,[∥,@]
Aline Gomez Maqueo Chew,[∥] Francesco Buda,[†] Donald A. Bryant,[∥] Alfred R. Holzwarth,[‡]
and Huub J. M. de Groot*,[†]

[†]Leiden Institute of Chemistry, Leiden University, P.O. Box 9502, 2300 RA Leiden, The Netherlands
[‡]Groningen Biomolecular Sciences and Biotechnology Institute, 9747 AG Groningen, The Netherlands
[§]Max-Planck-Institut für Bioanorganische Chemie, D-45470 Mülheim a. d. Ruhr, Germany
[∥]Department of Biochemistry and Molecular Biology, The Pennsylvania State University, University Park, Pennsylvania 16802, United States

ⓢ *Supporting Information*

ABSTRACT: The self-aggregated state of bacteriochlorophyll (BChl) *c* molecules in chlorosomes belonging to a *bchQ bchR* mutant of the green sulfur bacteria *Chlorobaculum tepidum*, which mostly produces a single 17^2-farnesyl-(R)-[8-ethyl,12-methyl]BChl *c* homologue, was characterized by solid-state nuclear magnetic resonance (NMR) spectroscopy and high-resolution electron microscopy. A nearly complete ^{1}H and ^{13}C chemical shift assignment was obtained from well-resolved homonuclear ^{13}C–^{13}C and heteronuclear ^{1}H–^{13}C NMR data sets collected from ^{13}C-enriched chlorosome preparations. Pronounced doubling (1:1) of specific ^{13}C and ^{1}H resonances revealed the presence of two distinct and nonequivalent BChl *c* components, attributed to all *syn*- and all *anti*-coordinated parallel stacks, depending on the rotation of the macrocycle with respect to the 3^1-methyl group. Steric hindrance from the 20-methyl functionality induces structural differences between the *syn* and *anti* forms. A weak but significant and reproducible reflection at $1/0.69$ nm^{-1} in the direction perpendicular to the curvature of cylindrical segments observed with electron microscopy also suggests parallel stacking of BChl *c* molecules, though the observed lamellar spacing of 2.4 nm suggests weaker packing than for wild-type chlorosomes. We propose that relaxation of the pseudosymmetry observed for the wild type and a related BChl *d* mutant leads to extended domains of alternating *syn* and *anti* stacks in the *bchQ bchR* chlorosomes. Domains can be joined to form cylinders by helical *syn–anti* transition trajectories. The phase separation in domains on the cylindrical surface represents a basic mechanism for establishing suprastructural heterogeneity in an otherwise uniform supramolecular scaffolding framework that is well-ordered at the molecular level.
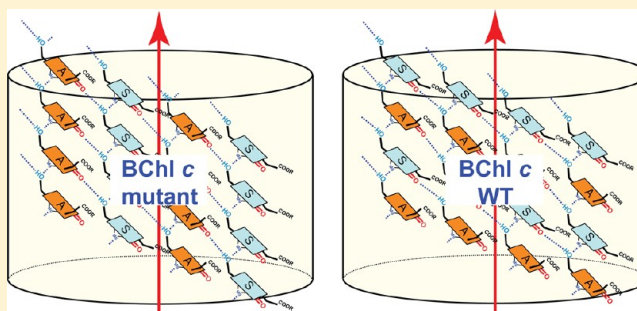
Green bacteria make up a group of organisms that often live in extremely low-light environments, such as at depths of 100 m in the Black Sea.[1] The ability to capture light energy and rapidly deliver it to photosynthetic reaction centers is essential to these bacteria, some of which see only a few photons of light per chlorophyll per day. To achieve this, the bacteria produce heterogeneous structures called chlorosomes, which differ from other antenna complexes by their very large size (~150 nm × 60 nm) and the absence of a protein matrix to support and organize the photosynthetic pigments.[2−5] Chlorosomes can form under extreme environmental conditions and allow for photosynthesis at extraordinarily low light intensities by the ultrarapid transfer of energy to their photosynthetic reaction centers.[6−8] They are remarkably stable against photodegradation because of self-protection of the BChls from triplet and singlet oxygen formation.[2,9] The unique optical and excitonic properties of chlorosomes have not been found in any other material, and chlorosomes may thus provide a paradigm for the rational design of biomimetic, self-assembling, and self-repairing structures for artificial photosynthesis and molecular electronics.[10−12]

The chlorosomes in green bacteria have been the last class of light-harvesting complexes to be characterized structurally. Chlorosomes are assembled from BChl *c*, *d*, or *e* and contain naturally heterogeneous molecular mixtures of BChls with different side chain modifications and stereochemistry. Up to 250000 BChls are self-organized into supramolecular, light-harvesting organelles, which have strongly red-shifted absorption bands and extremely large exciton diffusion lengths. The latter are thought to cover minimally ~10 and 20 BChl

monomers, which have been inferred as the delocalization lengths in chlorosomes and in artificial aggregates, respectively.[7,13] Each chlorosome has a unique structural organization,[14] and this variability in size, composition, and structure makes the chlorosomes unsuitable for X-ray crystallography. To circumvent this problem, we developed a dedicated approach by combining genetic techniques to create mutants of *Chlorobaculum tepidum* with a more homogeneous BChl distribution, cryo-electron microscopy (EM) to identify the larger distance constraints for BChls in the chlorosome, solid-state nuclear magnetic resonance (NMR) spectroscopy to determine the structure of the BChl molecules, and molecular modeling to combine all pieces of information into a single structure. This led to a detailed "template" microstructure and suprastructure for a well-characterized *bchQ bchR bchU* (hereafter *bchQRU*) *C. tepidum* triple mutant, which produces chlorosomes with strongly reduced variability, because the self-assembled BChl *d* molecules in these chlorosomes form very homogeneous, extended domains that are highly ordered at length scales of 1–100 nm.[5] NMR distance constraints and ring current analyses revealed *syn–anti* dimer stacks having alternating molecular conformations of the 3^1 side chain, while cryo-EM images and their Fourier transforms showed that the stacks were oriented almost perpendicular to the tube axis, forming shallow helices that self-assembled into sheets and concentric nanotubes with lamellar spacings of 2.15 nm.[5]

The *bchQRU* mutant synthesizes almost exclusively 17^2-farnesyl-(*R*)-[E,M]BChl *d*, and there is pseudosymmetry in the template structure around each BChl. The alternating rotation of the macrocycle with respect to the 3^1-methyl group is necessary for the realization of the template, while the other major asymmetry, the stereochemistry at positions 17 and 18, determines the sign of the helicity within the same template model.[5] The *bchQRU* mutant produces only one predominant signal component in the NMR, representing ∼90% of the spectral intensity, while a strong layer line occurs in the Fourier transform of the cryo-EM images.[5] In contrast, the WT contains a complex mixture of BChl *c* molecules that are sterically crowded and heterogeneous in the side chain functionalities of the chlorin rings, with variable degrees of methylation at 8^2-C and 12^1-C, and both *R* and *S* chirality at the 3^1-C.[2,15,16] The layer line in the cryo-EM was weak and revealed *syn–anti* dimer stacking parallel to the tube axis.[5] We observed a pronounced splitting of signals in the NMR, with two signal components in a 7:3 ratio,[17] each of them well-ordered on a local scale. Thus, for a considerable fraction of the BChl *c* in the WT chlorosomes, full pseudosymmetry associated with *syn–anti* pairs in spatially extended domains was not established, and the periodicity in the suprastructure of the WT was found to be much less extended than for the *bchQRU* mutant. It is interesting, however, that a more stringent control of the growth and isolation procedures recently gave rise to a structurally highly homogeneous preparation, as evidenced by single-chlorosome fluorescence polarization spectroscopy.[18]

In this work, variability due to two distinct modes of cooperative self-assembly was resolved by magic-angle-spinning (MAS) NMR analyses of chlorosomes of a *bchQ bchR* (hereafter *bchQR*) double mutant of *C. tepidum*. The data suggest that the chlorosomes from the *bchQR* mutant of *C. tepidum*, which synthesizes almost exclusively 17^2-farnesyl-(*R*)-[E,M]BChl *c*, differ from the WT and the *bchQRU* triple mutant and consist of domains comprised of parallel-stacked *syn*- and *anti*-coordinated molecules. The domains can be

joined with helical *syn–anti* transition regions to produce cylindrical structures with heterogeneity at the supramolecular level.

■ MATERIALS AND METHODS

Sample Preparation. Cells of the *C. tepidum bchQR* double mutant strain described by Gomez Maqueo Chew et al.[15] were grown as described by Balaban et al.[16] Cultures were grown in batch mode in 1.5 L fermentation bottles with continuous slow stirring at 40 °C. Growth light was controlled at the surface of the bottles (25 μE m^{-2} s^{-1} PAR) provided by two 40 W fluorescent neon tubes. Cells uniformly labeled with ^{13}C were obtained in steps. First, a 50 mL inoculum of cells grown in Wahlund medium was inoculated into 1 L of Wahlund medium without acetate.[19] In the next step, a 50 ml cell inoculum obtained from the acetate-free culture was inoculated into Wahlund medium (1 L) containing sodium [^{13}C]bicarbonate as the sole carbon source and [^{15}N]-ammonium chloride as the sole nitrogen source (Campro Scientific). The other source of N and C for the medium, ammonium acetate, was not used; the ammonium was adjusted with a larger amount of [^{15}N]ammonium chloride, while the total carbon concentration was adjusted by using a higher concentration of sodium [^{13}C]bicarbonate. Cells were grown for 3 days and then harvested by centrifugation. Chlorosomes were isolated as described in detail by Balaban et al.[16] and Oostergetel et al.[14] and were kept in the dark at ∼4 °C prior to the collection of NMR data. The pigments from the *bchQR* mutant were also isolated and analyzed following the methods described by Steensgaard et al.,[20] and more than 95% of the total BChl was 17^2-farnesyl-(*R*)-[8-ethyl,12-methyl]BChl *c*.

NMR Measurements. All solid-state, MAS NMR experiments were performed with a Bruker AV-750 spectrometer equipped with a 4 mm triple-resonance MAS probe head (Bruker, Karlsruhe, Germany), using a ^{13}C radiofrequency of 188.6 MHz and a sample temperature of 277 K. Spinning frequencies of 11 kHz ± 5 Hz and 13 kHz ± 5 Hz were used for two-dimensional (2D) ^{13}C–^{13}C homonuclear and ^{1}H–^{13}C heteronuclear correlation experiments, respectively. The ^{1}H magnetic moments were decoupled during acquisition using the two-pulse phase modulation (TPPM) scheme[21] in all experiments. 2D ^{13}C–^{13}C dipolar correlation spectra were recorded using the radiofrequency-driven, dipolar recoupling (RFDR) sequence with phase-sensitive detection in ω_1 with mixing times of 1.4, 2.9, and 5.1 ms.[22] A ^{1}H $\pi/2$ pulse length of 3.1 μs was used with cross-polarization periods of 2 ms. For each of the 256 steps in the indirect dimension, 128 scans were collected. 2D ^{13}C–^{13}C spectra were recorded using the CHHC/CP[3] sequence for indirect detection of ^{1}H–^{1}H contacts with ^{1}H diffusion times of 250 μs for the *bchQR* chlorosomes and 300 and 400 μs for the WT chlorosomes.[23,24] The initial CP contact time was set to 256 μs. Short CP contact times of 128 μs enclosing the ^{1}H–^{1}H spin diffusion step were used to ensure that the polarization transfer was restricted to directly bonded ^{1}H–^{13}C spin pairs. For each of the 256 steps in the indirect dimension, 128 scans were collected. 2D ^{1}H–^{13}C heteronuclear correlation data were collected using the frequency-switched Lee–Goldburg (FSLG) experiment,[25] with a short CP time of 256 μs and a ^{1}H 90° pulse of 3.1 μs (Figure 1). The ^{1}H chemical shift scale was calibrated from a FSLG spectrum of solid tyrosine hydrochloride salt. For each of the 128 steps in the indirect ^{1}H dimension, 128 ^{13}C scans were collected. One-dimensional (1D) ^{15}N CP/MAS experiments
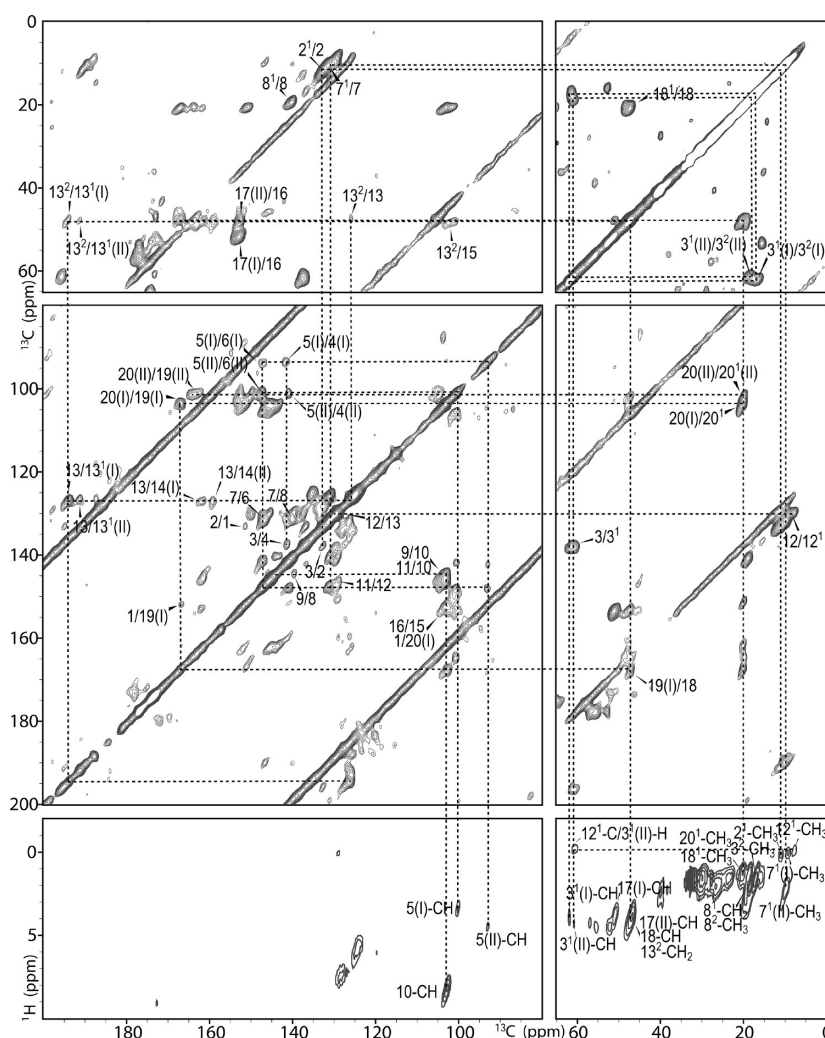
Figure 1. Contour plot sections of a ^{13}C−^{13}C MAS NMR dipolar correlation spectrum of chlorosomes from the *bchQR* mutant recorded in a field of 17.6 T using a spinning frequency of 11 kHz and a mixing time of 1.4 ms. The bottom panels show contour plot sections of a ^{1}H−^{13}C MAS NMR FSLG dipolar correlation spectrum recorded in the same field employing a spinning rate of 13 kHz. The FSLG panels are plotted at different contour levels. The ^{13}C−^{13}C and ^{1}H−^{13}C connectivity networks are indicated with dashed lines, and the two spectral components are numbered I and II.

were performed on both samples, leading to the accumulation 86000 scans with variable-amplitude CP periods of 5.12 ms. The ^{15}N resonances were referenced to liquid NH$_3$.

^{13}C and ^{1}H shifts in solution (σ_{liq}^{C} and σ_{liq}^{H}, respectively) were determined with 2D ^{13}C−^{13}C COSY, ^{1}H−^{1}H COSY, and ^{1}H−^{13}C HSQC NMR spectra of the monomer in CD$_2$Cl$_2$ with 5% CD$_3$OD recorded on a DMX-600 spectrometer (Bruker).

Cryo-Electron Microscopy. Aliquots of purified chlorosomes were applied to holey carbon grids with a thin layer of carbon and were plunge-frozen in liquid ethane at 83 K with a Vitrobot vitrification system (FEI, Eindhoven, The Netherlands). Electron microscopy was performed with a Tecnai G2 Polara electron microscope (FEI) equipped with a Gatan energy filter at 115000× magnification and a specimen temperature of 80 K. Images were recorded in the zero-loss imaging mode, using a slit width of 20 eV, with a slow-scan CCD camera at 1 μm underfocus, to have optimal phase contrast transfer at 300 kV for details with a periodicity of ∼2 nm.

Structural Modeling and Calculations. BChl *c* monomers axially coordinated to a methanol molecule in the *syn* and *anti* configurations were geometry optimized from first

principles. Density functional theory (DFT) calculations were performed using Gaussian 03 and the Becke, Lee, Yang, and Parr (BLYP) exchange-correlation functional, which has been used previously to estimate NMR shifts for (B)Chl systems.[26−29] The 6-311++G(d,p) Gaussian basis set was used. NMR shifts were calculated using the Gauge-Independent Atomic Orbital (GIAO) method.[30−32] The six out-of-plane normal deformations of the saddling (sad, B$_{2u}$), ruffling (ruf, B$_{1u}$), doming (dom, A$_{2u}$), waving [wav(x) and wav(y), E$_g$], and propellering (pro, A$_{1u}$) types were calculated for each of these monomers in the lowest-frequency mode using the NSD program (available online), which was developed by the group of Shelnutt and co-workers.[33,34] Tubular models comprising alternating all-*syn* and all-*anti* stacks were built in Swiss PDB viewer.[35] EM images were simulated from these models as projected electron density from the atomic coordinates at 0.6 nm resolution using EMAN pdb2mrc.[36]

■ RESULTS AND DISCUSSION

Chemical Shift Assignment. The ^{13}C and ^{1}H chemical shift assignments of the BChls in chlorosomes from the *bchQR* mutant were obtained from well-resolved, 2D homonuclear
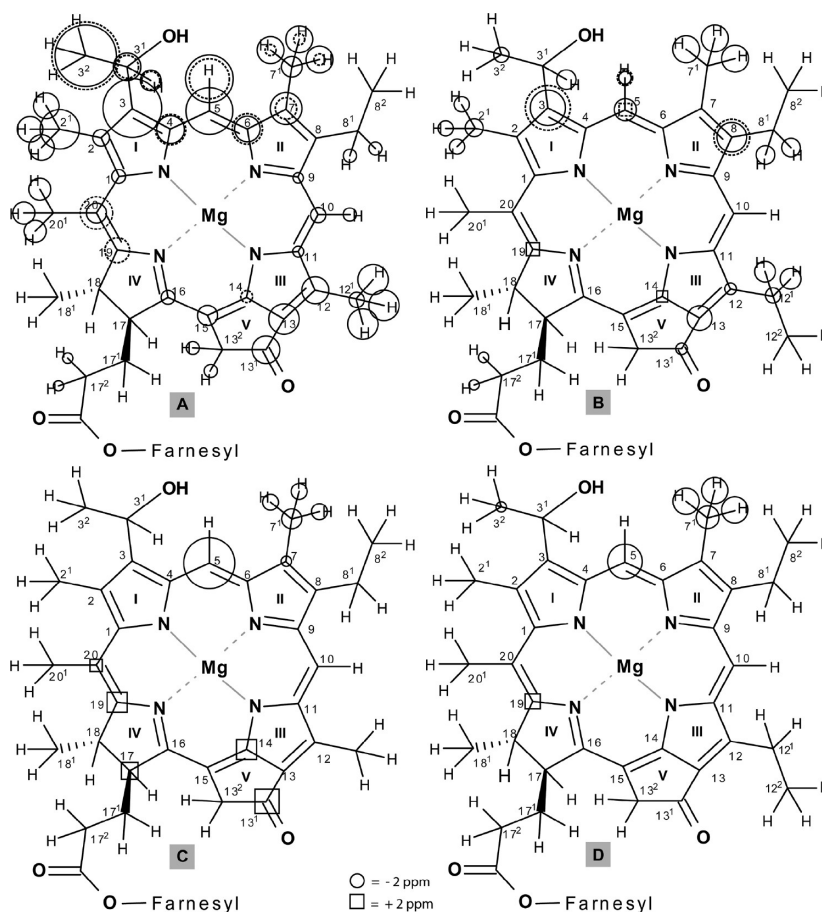
Figure 2. (A and B) Observed ^{1}H and ^{13}C aggregation shifts of chlorosomes from the (A) *bchQR* mutant and (B) WT of *C. tepidum* for values of no less than |±1.5| ppm. The aggregation shifts of components I and II are plotted as solid and dashed circles, respectively. (C and D) Differences in ^{13}C chemical shifts between components I and II of the chlorosomes from the (C) *bchQR* mutant and (D) WT for $\Delta\sigma_i$ values of no less than |±1.5| ppm. The size of the circle/square is proportional to the magnitude of the shift.

^{13}C−^{13}C and heteronuclear ^{1}H−^{13}C dipolar correlation data sets, which are shown in the composite plot in Figure 1. The nearest-neighbor connectivity in the molecular network leading to the assignment of BChl *c* in chlorosomes is indicated with dashed lines. The lines were very narrow, ∼1−2 ppm, reflecting a high degree of local order for the BChl *c* molecules in the *bchQR* mutant. The RFDR spectra recorded for the chlorosomes from WT *C. tepidum*, with mixing times of 1.4 and 2.9 ms (data not shown), had a resolution better than that of previously reported data measured at a lower field.[16,37] The resolution of the data collected from *bchQR* chlorosomes remained superior, however, revealing more homogeneous and probably tighter packing of the BChl *c* molecules in the mutant chlorosomes relative to the WT. This difference is attributed to the presence of a single 17^2-farnesyl-(*R*)-[E,M]BChl *c* homologue in the mutant and a complex and heterogeneous mixture of BChl *c* homologues in the WT. The variable degrees of methylation at 8^2-C and 12^1-C, and both *R* and *S* chirality at 3^1-C, most likely lead to structural disorder that translates into inhomogeneous line broadening. The ^{13}C chemical shift assignment for chlorosomes from the WT agreed well with the data reported by Balaban and co-workers.[16]

For chlorosomes from the *bchQR* mutant, doubling of signals was observed for the ^{13}C resonances from positions 3^1-C, 3^2-C, 4-C, 5-C, 6-C, 7-C, 7^1-C, 13^1-C, 14-C, 17-C, 19-C, and 20-C of the BChl *c* ring. This led to two correlation networks, denoted

as components I and II. Two components were also observed with WT chlorosomes for ^{13}C resonances at all positions seen for the *bchQR* mutant except at 13^1-C, 14-C, and 20^1-C, and additional doubling was observed at positions 8-C and 16-C. In the ^{1}H−^{13}C data for the mutant, the 3^1-H, 5-H, 7^1-H$_3$, and 17-H correlation signals that arise from protons directly bonded to carbons with doubled resonances are split in the ^{1}H dimension as well. The differences in ^{1}H chemical shifts between components I and II are generally <1 ppm, except for that of 7^1-H$_3$ (2−4 ppm), and were small compared to the differences of 2−5 ppm in their ^{13}C chemical shifts. Because the ^{13}C shifts are very sensitive to the molecular conformation and the ^{1}H shifts are primarily due to ring currents from adjacent molecules, the NMR data revealed two distinct conformers with similar stacking modes.

The ^{13}C (σ_I^C/σ_{II}^C) shifts for the two signal components and the ^{1}H (σ_I^H) shifts for the major component in the data sets collected from *bchQR* and WT chlorosome samples are summarized in Tables S1 and S2 of the Supporting Information. The chemical shifts were used to calculate the aggregation shifts: $\Delta\sigma_i^C = \sigma_i^C - \sigma_{liq}^C$ and $\Delta\sigma_i^H = \sigma_i^H - \sigma_{liq}^H$ for ^{13}C and ^{1}H, respectively. The aggregation shifts for components I and II for chlorosomes from the *bchQR* mutant and the WT are plotted in panels A and B of Figure 2. In the *bchQR* mutant chlorosomes, 3^2-C showed an anomalously large aggregation shift of −8.9 ppm, which was not mirrored in the 3^2-H$_3$ shifts. We observed upfield shifts larger than those reported in

previously published data at positions 8^1-H_2 and 17^2-H_2, and downfield shifts at positions 14-C and 19-C, for component I of the WT.[17] The difference in chemical shifts between the two components was plotted in panels C and D of Figure 2 for *bchQR* and WT, respectively, in which the radii of the circles denote the magnitudes of the differences.[38] Previously, four possible self-assembly modes were identified for the BChls: the parallel stack, the piggyback dimer, the antiparallel monomer stack, and the *syn−anti* dimer stack.[5] The $\Delta\sigma_i^H$ for the *bchQR* mutant chlorosomes are all less than 7 ppm. This effectively excludes the piggyback dimer and antiparallel monomer stacking modes, which should give rise to pronounced $\Delta\sigma_i^H$ of >7 ppm for protons around ring I or ring II because of overlap with adjacent BChls on both sides of the molecular plane.[5]

The 1D ^{15}N CP/MAS spectra for chlorosomes from the *bchQR* mutant and the WT are shown in Figure 3. The signals
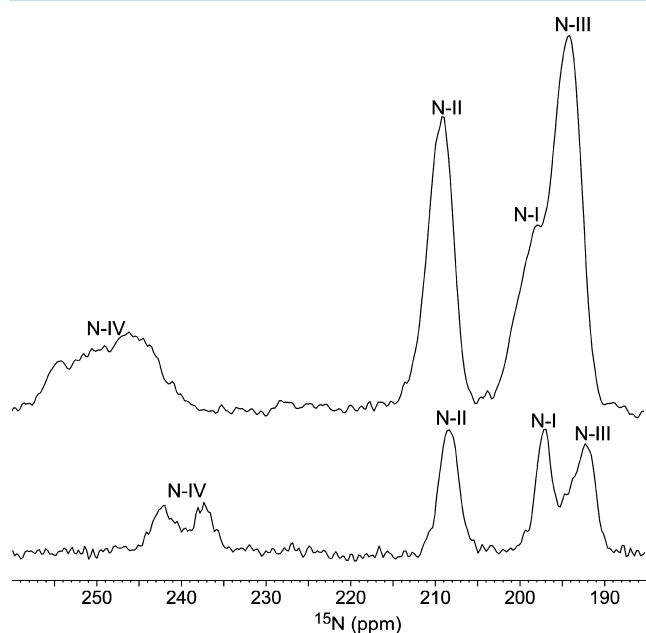
and the peak with less intensity was shifted by 5.7 ppm. The signals for N-I and N-III were well separated in the mutant, and the signal for N-III is relatively broadly dispersed, most probably over more than two components. N-I and N-III overlap in the WT spectrum. The response from N-IV was distributed over two well-resolved peaks of almost equal intensity at 237.3 and 242.0 ppm for chlorosomes from the *bchQR* mutant, similar to what was observed for solid 17^2-farnesyl-(R)-[E,E]BChl c aggregates.[40] In contrast, for the WT, a broad N-IV response was dispersed over a range from 240 to 255 ppm. Using Gaussian deconvolution, it could be decomposed into three overlapping components at 246.1, 248.9, and 254.2 ppm, with an intensity ratio of 4.0:3.5:2.5. The ^{15}N chemical shifts are listed in Table 1.

Distance Constraints. To proceed from the NMR chemical shift data into the structure at the molecular level, proton-mediated correlation spectroscopy with short mixing times of 250−400 μs was used.[41] The correlations depicted in Figure 4 belong to the *bchQR* mutant and were derived from a

Figure 3. 1D CP/MAS ^{15}N spectrum for uniformly ^{13}C- and ^{15}N-enriched chlorosomes from the *bchQR* mutant (bottom trace) and WT (top trace) of *C. tepidum* recorded in a field of 17.6T at a 12 kHz MAS frequency. The CP contact time was set to 5.12 ms; 86000 scans were collected with a recycle delay of 2 s.
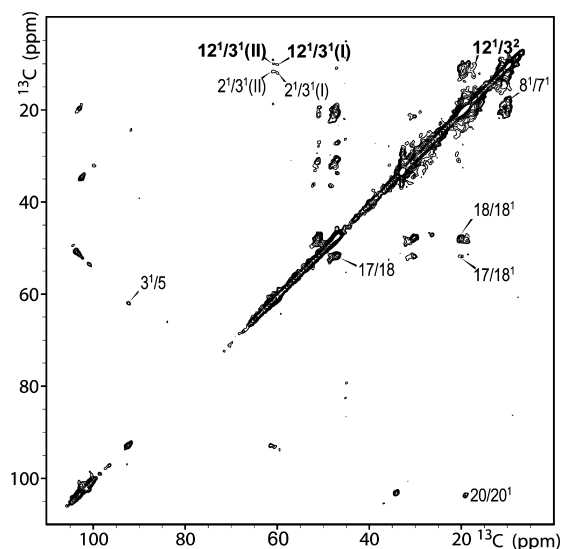

Figure 4. ^{13}C−^{13}C CHHC data sets of chlorosomes from the *bchQR* mutant of *C. tepidum* recorded in a field of 17.6 T using spinning frequencies of 13 kHz. A ^{1}H−^{1}H spin diffusion mixing time of 250 μs was used. The correlations labeled in boldface were identified as intermolecular.

have been assigned by comparison with data for monomeric BChl c in solution.[39] The chemical shifts for N-I, N-II, and N-III were close to the reported solution shifts. The signals for N-IV in the *bchQR* mutant were shifted with respect to the solution response by −11.2 and −6.5 ppm, while for the WT chlorosomes, the stronger response was shifted by −2.4 ppm

data set collected with a short CHHC mixing time of 250 μs. These correlations originate between nearby substituents of BChl c molecules in the mutant chlorosomes and represent ^{1}H−^{1}H distances of less than ∼3 Å, in agreement with the proton transfer range previously established for this experiment.[41−43] The $12^1/3^1$ and $12^1/3^2$ cross-peaks represent intermolecular contacts, while the $2^1/3^1$, $3^1/5$, 20/20^1, 17/18,

Table 1. Assignment of ^{15}N Chemical Shifts of BChl c from Chlorosomes of the *bchQR* Mutant and WT Strains of *C. tepidum*

position	monomer[a]	BChl c aggregate[b]		*bchQR*		WT	
		type A	type B	I	II	I	II
N-I	197.4	197.7	195.7	197.0		197.8	
N-II	209.7	209.8	208	208.4		209.0	
N-III	193.7	194.8		192.3	194.6	194.1	
N-IV	248.5	247.5	254.5	237.3	242.0	246.1, 248.9	254.2

[a]Monomer shifts for (3^1R)-[E,E]BChl c_F in acetone-d_6.[39,40] [b](3^1R)-[E,E]BChl c_F in solid aggregates treated in CH_2Cl_2.[40]

Table 2. Out-of-Plane Distortions of the Lowest-Frequency Mode for Geometry-Optimized Structures of Noncoordinated, 3^1-R and -S, *syn*-Coordinated, and *anti*-Coordinated [8-Me,12-Me]BChl *c* Using Normal-Coordinate Structural Decomposition[a]

| | out-of-plane displacement (Å) | | | | | | | |
| | total distortion | | B_{2u} | B_{1u} | A_{2u} | $E_g(x)$ | $E_g(y)$ | A_{1u} |
BChl *c*	d_{obs}	δ	d_{sad}	d_{ruf}	d_{dom}	$d_{wav(x)}$	$d_{wav(y)}$	d_{pro}
3^1-*R*-*anti*	1.723	0.220	1.094	0.814	0.871	−0.069	0.296	−0.509
3^1-*R*-*syn*	1.503	0.183	0.893	0.459	0.701	−0.287	0.481	−0.667

[a]The observed total distortions (d_{obs}), as well as the corresponding standard deviation (δ), are also listed.

$17/18^1$, $18/18^1$, and $8^1/7^1$ cross-peaks represent intramolecular contacts. Intermolecular correlations between carbons 12^1 and 3^1 and carbons 12^1 and 3^2 were detected between rings I and III of two BChl *c* molecules from adjacent stacks, which is consistent with a parallel stacking motif. The $12^1/3^1$ intermolecular correlations were also observed, which correspond to components I and II of 3^1. This was attributed to the presence of two different conformations of the 3^1 side chain that can arise from BChls that are coordinated in a *syn* or an *anti* orientation.

Ring Deformation. Two geometry-optimized molecules of 17^2-methyl-(*R*)-[E,M]BChl *c*, one of which was *syn*-coordinated and the other *anti*-coordinated to a methanol molecule, were analyzed with NSD to estimate the extent of nonplanarity of the macrocycle in the two forms at the monomer level and how this affects the chemical shifts. The ring deformations in the lowest-frequency normal modes are listed in Table 2.[33] The *anti*-coordinated BChl *c* showed a pronounced saddling with additional doming and ruffling displacement. The *syn*-coordinated BChl *c* showed less overall displacement than the *anti*-coordinated molecule, especially for the ruffling component.

Out-of-plane distortions have an effect on the metal–nitrogen distances, and ab initio quantum-chemical calculations and solid-state NMR studies on metal–tetraphenylporphyrin compounds indicate that the ^{15}N chemical shifts tend to be determined by the metal–nitrogen separation.[33,44] The long farnesyl tail on ring IV lies on the same side as the coordinate bond of Mg for a *syn*-coordinated molecule, while it lies on the opposite side of the coordinate bond in an *anti*-coordinated molecule.[45] It is at the edge of a range of steric crowding that extends from ring IV to ring I and involves the 18^1-, 20^1-, and 2^1-methyl groups. However, ring IV is saturated at carbons 17 and 18 and asymmetric, which makes it a "weak spot" and more susceptible to adaptation to N–Mg coordination changes and the accommodation of steric hindrance than ring I and the other two rings, which are unsaturated and therefore more rigid. The calculated overall distortion of the 17^2-methyl-(*R*)-[E,M]BChl *c* model that is *anti*-coordinated differed from the *syn*-coordinated BChl *c* molecule by ∼0.2 Å (Table 2). Two distinct N-IV peaks of almost equal intensity were seen for the chlorosomes of the *bchQR* mutant. These peaks can be reconciled with the presence of equal amounts of *syn*- and *anti*-coordinated BChl *c*. The broad response seen for N-IV in the WT chlorosomes is more difficult to rationalize because of the presence of bulkier groups at positions 8^2-C and 12^1-C. The intensity ratio of the N-IV peaks was seen to be 4:3.5:2.5, which suggested that for the WT chlorosomes ring deformation is a complex process determined by more than one factor, such as the different side chains at positions 8^2-C and 12^1-C and chirality at 3^1-C. For the WT, ^{25}Mg NMR spectroscopy revealed a pair of signals with different quadrupole couplings,

which confirmed the occurrence of two different surroundings for the central metal ion.[46] Such differences can originate from the interactions between stacks. From studies of artificial BChl mimics, it has been deduced that it is the increased π–π overlap with an increase in aggregate size that leads to an energetically cooperative stabilization mechanism.[47] In contrast, although the electrostatic contribution to the total energy is the most dominant one, it increases linearly with aggregation and does not contribute to the increased level of stabilization of the aggregates.[47] Thus, under different stacking conditions, polymorphism in the molecular arrangement is possible from competing interactions in the Mg−OH···O=C structural motif involving differences in hydrogen bonding between the stacks and the positioning of the ring V keto functionality from an adjacent stack.[48] Similar phenomena of polymorphism are well-known for other pigment aggregates, for example, in structurally related phthalocyanine pigments.[49]

Spectral Doubling. To resolve the possible sources of doubling observed in the ^{13}C and ^{15}N NMR data sets of the chlorosomes from the *bchQR* mutant, chemical shifts were calculated for the optimized *syn*-coordinated and *anti*-coordinated BChl *c* monomer models with DFT methods (Figure 5). Significant doublings are calculated for positions 17-C, 19-C, and 20-C from structural differences due to *syn* and *anti* coordination for BChl *c* monomers. The sign and magnitude are consistent with the doubling of resonance signals around ring IV detected with NMR for chlorosomes
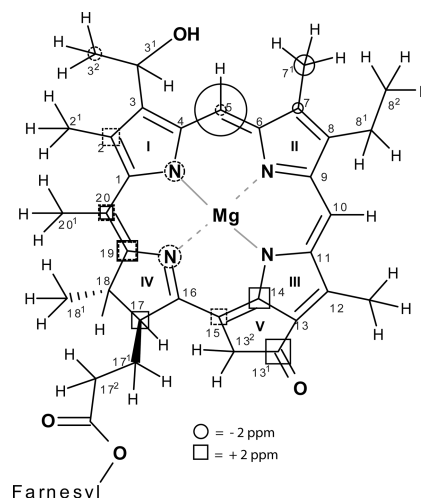

Figure 5. Differences in the calculated chemical shifts of geometry-optimized *syn*- and *anti*-coordinated BChl *c* monomers plotted as dashed circles and squares. The experimental differences between components I and II for the *bchQR* mutant are shown as solid circles and squares. Differences of more than |±1.5| ppm are indicated. The sizes of the circles and squares are proportional to the magnitudes of the shifts.
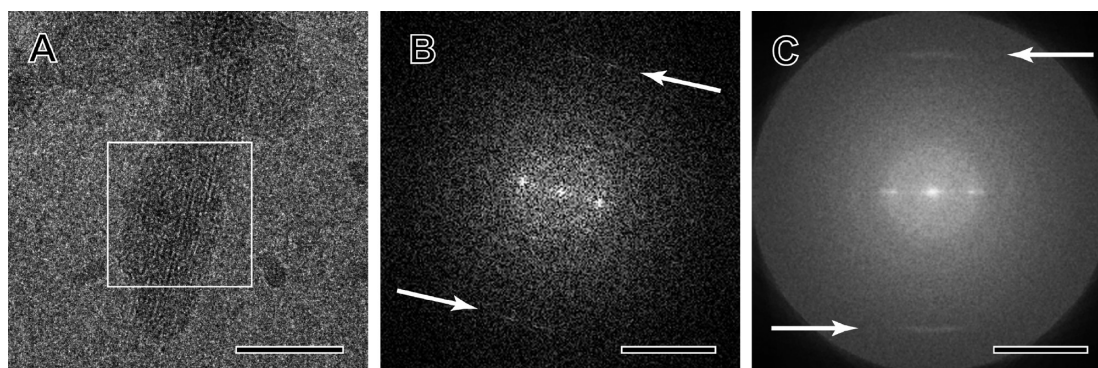
Figure 6. Cryo-electron microscopy of *bchQR* mutant chlorosomes. (A) Electron micrograph of an unstained, frozen, hydrated chlorosome. Striations are from the lamellar spacing of 2.4 nm. The bar is 50 nm. (B) Fourier transform calculated from the boxed area in panel A. White arrows indicate the layer line at $(1/0.69)$ nm^{-1} from the monomer stacking. The bar is 1 nm^{-1}. (C) Sum of 23 aligned Fourier transforms of chlorosome micrographs, similar to the image shown in panel A, which enhances the visibility of the layer line intensity. The bar is 1 nm^{-1}.

from the *bchQR* mutant, which corroborates the evidence of the presence of both *syn*- and *anti*-coordinated molecules in the suprastructure. While *syn*-coordinated BChl *c* and *anti*-coordinated BChl *c* are moderately different in their chlorin rings, and the overall distortion of a BChl *c* molecule that is *anti*-coordinated differs from that of a *syn*-coordinated BChl *c* molecule by ~0.2 Å, cooperative self-assembly of only *syn*-BChl *c* or only *anti*-BChl *c* driven by increased $\pi-\pi$ overlap can be expected to amplify or quench these differences, depending on the size of the enthalpy and combinatorial entropy terms that determine the free energy balance in the thermodynamics of the self-assembly process. For the chlorosomes of the *bchQR* mutant, the microscopic stabilization terms are apparently dominant and lead to phase separation in the suprastructure with two stacking modes that give rise to enhanced distortions at the molecular level, with different chemical shifts at many positions of the bacteriochlorin rings. This is in agreement with the large ^{13}C aggregation shifts over a large part of the ring observed in the homonuclear ^{13}C correlation data set in Figure 1. The resonance observed at 5-C gives a chemical shift of 93.5 ppm for component I (Table S1 of the Supporting Information), which differs substantially from the values of 97.0 ppm observed for the WT (Table S1 of the Supporting Information) and 97.2 ppm observed for the *bchQRU* mutant.[5] A crucial element is the magnitude of these carbon aggregation shifts. For the *bchQRU* mutant and the WT, 5-C is only slightly shifted, while for the BChls in chlorosomes of the *bchQR* mutant, it is more shifted. This means that the average amplitude of the difference between the two components is larger in the chlorosomes of the *bchQR* mutant than for the other two. Thus, when the macrocycles are oscillating in their normal modes, this flexibility makes it easy for the suprastructure to shape the monomers for optimal self-assembly. In the *bchQRU* chlorosomes, the suprastructure is dominant, and there is only one average structure of the ring, in which the ring is alternating in a *syn* and *anti* orientation with respect to the 3^1-C side chain.

Structural Assessment of the Mutant versus the WT. The Q$_y$ absorption band of the BChls in chlorosomes of the *bchQR* mutant has a half-bandwidth that is much narrower than that of the WT.[15] This limits the range of available wavelengths of light in the far-red region that can be utilized by the mutant, thereby significantly reducing the light-harvesting potential.[15] Hence, the doubling into two well-defined structural regions that is inferred from the NMR data and modeling leads to a

BChl organization in chlorosomes that is not optimal for light harvesting. The inhomogeneous broadening is reduced because of the absence of varied methylation at 8^2-C and 12^1-C. Moreover, it is likely that all-*syn* and all-*anti* stacking is more uniform; this would lead to less static and dynamic heterogeneity with narrower distributions of site energies for the BChls. In addition, the observation that *bchQR* mutant chlorosomes are built of domains with cylindrical structures in different orientations is mainly based on cryo-EM data (Figures S1 and S2 of the Supporting Information). The long-range lamellar repeats that are obvious in all of the chlorosomes of Figure S1 have previously been shown to arise from projections from the walls of cylindrical structures in Figure 4C,E of Ganapathy et al.[5] The domains themselves are internally rather well-ordered with a lamellar pattern similar to the BChl *c* molecules in chlorosomes of the *bchQRU* mutant, consistent with multilayer cylindrical structures (Figure 6A).[5] While the stacking of BChl appears to be tighter for the *bchQR* mutant than for the WT, the 2.4 nm spacing between layers in the electron micrographs for the *bchQR* mutant is larger than the 2.15 nm spacing observed for chlorosomes from the WT and the *bchQRU* mutant. This suggests a somewhat looser packing between lamellar surfaces for the *bchQR* species, which contains more carotenoids than the WT.[15] However, instead of the 1.22 nm repeat characteristic for *syn−anti* alternating stacking, a 0.69 nm spacing was reproducibly observed (Figure 6B,C). This is consistent with the monomer repeat in the all *syn*- and all *anti*-coordinated domains that is derived from the NMR analyses (see Figure 4). Both stacking modes detected by NMR can be interwoven into the same regular cylindrical array framework detected by the EM. This could provide an explanation for how heterogeneous structures can be formed, by joining extended domains with helical *syn−anti* interfaces that allow for a proper H-bonding alignment of ring V keto functionalities in a stack with the OH groups of an adjacent stack (for an example, see Figure 8C). Such arrangements lead to weak layer lines that we have consistently observed across chlorosomes containing different BChl species, while other three-dimensional packing reflections have never been observed.[5] From the line broadening of the 0.69 nm reflection, a correlation length on the order of ~30 nm is estimated for the best diffracting samples, which translates into an upper limit of ~40 monomer units between dislocations for the domains in the more regular chlorosomes. In contrast, structures without a regular cylindrical framework, such as undulating lamellae, would not
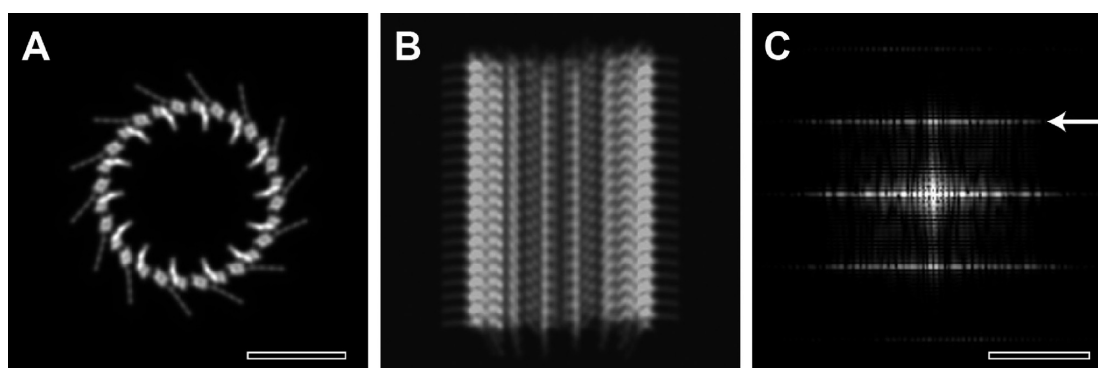
Figure 7. Electron microscopic image simulations for a tubular model comprising alternating all-*syn* and all-*anti* stacks. (A) Top view projection of the electron density, truncated at 0.6 nm resolution. The bar is 5 nm. (B) Side view projection. (C) Fourier transform of the image in panel B, showing a strong layer line at $1/0.69$ nm^{-1} (arrow). The bar is 2 nm^{-1}.
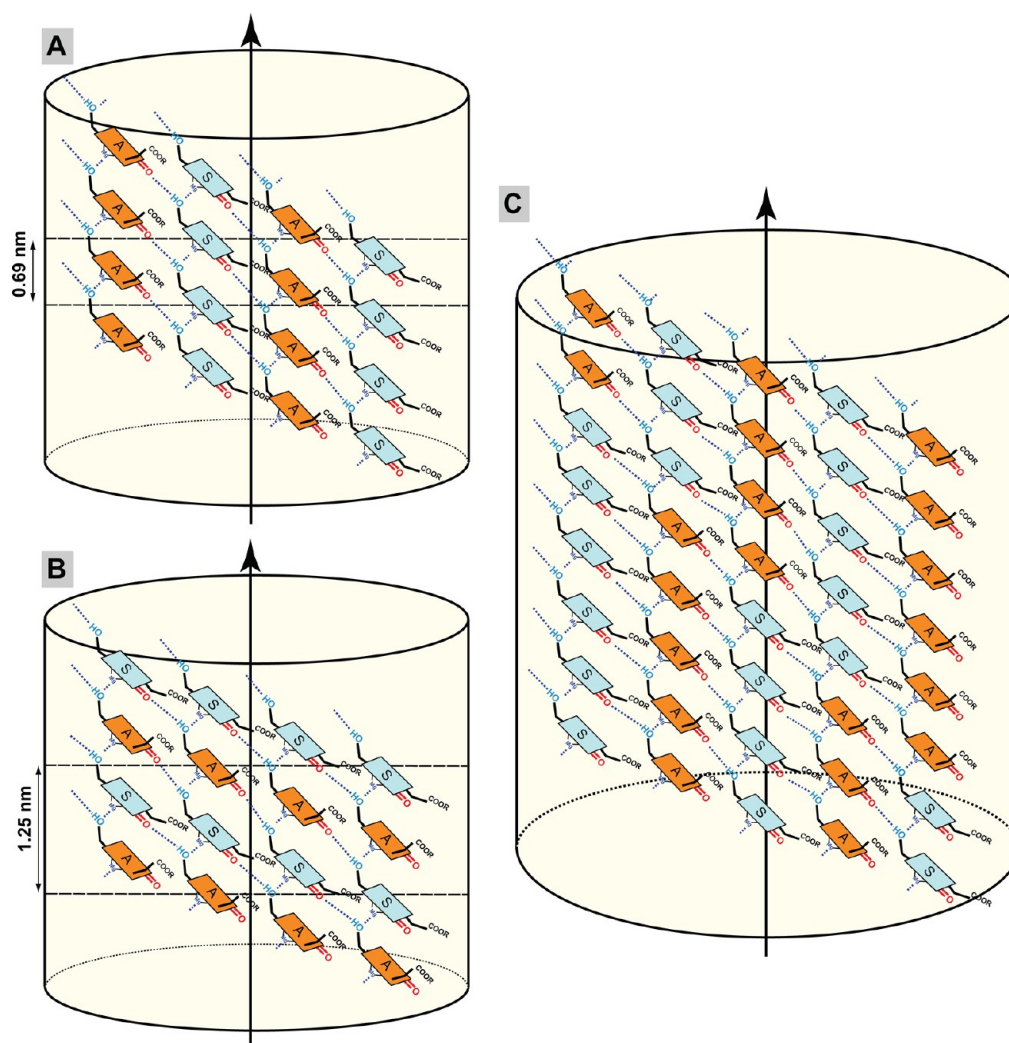

Figure 8. Schematic models of a section of the chlorosomal tube from the (A) *bchQR* mutant and (B) WT. Extended domains as in panel A can be joined by helical *syn*–*anti* interfaces to produce bulk heterogeneity in a highly regular tubular scaffold (C). Periodicities of 0.69 and 1.25 nm, respectively, are indicated. The arrows indicate the direction of the long axis of the chlorosome. A and S stand for BChl *c* molecules that are *syn*- and *anti*-coordinated, respectively.

produce a layer line and would give rise to excessive inhomogeneous line broadening in the NMR because of long-range bulk susceptibility effects.

Finally, our study emphasizes the roles that methylation at 8^2-C and 12^1-C plays in steering the self-assembly in chlorosomes. Nature clearly continued the evolutionary trajectory of BChl *c* to include the methylations at 8^2-C and 12^1-C. This means that the mixture of all-*syn* and all-*anti* parallel stacks determined here for the *bchQR* mutant was not optimal and that further improvements were selected by the

additional side chain methylation events to make a better light-harvesting antenna. For the WT chlorosomes, a separation into all *syn* and *anti* regions is apparently unfavorable, and instead, the BChls in chlorosomes form tubular supramolecular aggregates, for which the repeating unit along the stack is a *syn*−*anti* dimer with an ~1.22 nm repeat in the direction of the long axis. The tubular structure is sufficiently stable to support considerable heterogeneity at the molecular level and still produces a structure for optimal light-harvesting capacity.[2,50] Studies of BChls *c* aggregates in vitro have shown that varying degrees of methylation at positions 8^2 and 12^1 and the stereoisomeric configuration at position 3^1 influence the structure of the aggregates.[50−54] Gomez Maqueo Chew et al. have shown that the absorption spectrum of the *bchQR* double-mutant cells that produce 17^2-farnesyl-(*R*)-[E,M]BChl *c* differs from that of the related *bchQ* single mutant, which produces mostly 17^2-farnesyl-(*R*)-[E,E]BChl *c*. This suggests that aggregates of [E,M]BChl *c* may differ structurally from those of [E,E]BChl *c* in the mutant chlorosomes.[15] This is consistent with the dissimilarities in chemical shift and aggregation shift patterns that we have observed between chlorosomes from the *bchQR* mutant, which contain only [E,M]BChl *c*, and the WT, which contains more than 90% of [Pr,E]/[E,E]BChl *c*. This has led to an independent assessment of their structures. Thus, the stabilization of parallel stacking domains for the *bchQR* mutant contrasts with those of both the WT and the *bchQRU* mutant, in which the supramolecular self-organization is based on *syn*−*anti* stacks with pseudosymmetric BChl conformers because of dynamic adaptation of the macrocycle to the constraints imposed by the suprastructure. In the chlorosomes of the *bchQR* mutant, the inability of the molecular structure to dynamically adapt to establish pseudosymmetry leads to phase separation of *syn* and *anti* components, which condense into two tight parallel stacking modes with different macrocycle structures and considerable polymorphism. Most likely, all-*syn* and all-*anti* stacks alternate to form sheets and heterogeneous cylinder segments, in agreement with the 1:1 intensity ratio for the doubling in the spectra. Figure 7 shows a simulated electron micrographic image, calculated from a tubular model comprising alternating all-*syn* and all-*anti* stacks oriented in the direction of the tube axis. The calculated Fourier transform from the side view image displays a strong layer line at 1/0.69 nm^{-1}, arising from the monomer repeat and corresponding with experimental observations.

Chlorosomes are thought to be heterogeneous because of inherent frustration from the competition between cooperativity in π−π stacking interactions that promotes ordered domains in supramolecular tubular structures, and localized molecular interactions. The substantial variability in the structure of chlorosomes due to different distinct modes of cooperative self-assembly of slightly different BChls has been resolved by solid-state NMR analyses. This finding is of general interest because it provides major insights into the self-assembly process to build low-energy supramolecular aggregates. Apparently a small variation in the building blocks can give rise to substantially different structures. The *bchQR* mutant produces chlorosomes that predominantly contain a single 17^2-farnesyl-(*R*)-[E,M]BChl *c* homologue (>95%), without the complexity and heterogeneity of the BChls observed in the WT. On the other hand, the BChl *c* synthesized by this mutant is chemically more similar to the BChls of WT chlorosomes than the BChl *d* homologue that is synthesized by the *bchQRU* strain.[2,50] Distance constraints resolved from solid-state NMR

analyses performed on uniformly [13]C- and ^{15}N-enriched preparations of the *bchQR* chlorosomes revealed two parallel stacking components in the *bchQR* chlorosomes, illustrated schematically in Figure 8A, in contrast with the pseudosymmetric, alternating *syn*−*anti* main structural organization of the [E,M]BChl *d* in chlorosomes of the *bchQRU* strains, and the extended *syn*−*anti* regions that produce weakly observed layer lines in the EM data for the WT[5] depicted schematically in Figure 8B. For the *bchQR* chlorosomes, two sets of NMR signals were observed at specific positions on the BChl *c* ring, revealing two structural components in an approximately 1:1 ratio. The spectral doubling could be attributed to two similar but nonetheless different ring shapes, which correspond to extended domains of all *syn*-coordinated or all *anti*-coordinated molecules. For the *bchQR* mutant, steric hindrance involving the methyl group at the 20-*meso* position apparently affects the free energy landscape at the nanoscale and provokes symmetry breaking into extended *syn* or *anti* regions in a self-assembled 17^2-farnesyl-(*R*)-[E,M]BChl *c* homologue that propagates into the suprastructure. Cryo-EM images corroborated the presence of such parallel monomer stacking regions with a repeat of ~0.69 nm.

In conclusion, the common denominator in the suprastructures formed by BChls in chlorosomes of the WT and *bchQR* and *bchQRU* mutants is the parallel stacking of the BChl *c* or *d* homologues, with variations occurring because of the mixing or alternation of *syn* and *anti* ligation. In essence, this is "what makes a chlorosome a chlorosome", because it leads to the ferroelectric character that is found in no other antenna system. The suprastructure formed from the aggregated BChls allows for extensive delocalization of excitons by the enhanced charge transfer character in the excited state and can produce an extended dipole moment for rapid and efficient long-range energy transfer to the baseplate.[8,45,55] Although light harvesting occurs efficiently in chlorosomes containing [8-Et,12-Me]BChl *d* (the *bchQRU* mutant),[15] it is interesting to note that extension of the biosynthetic pathway to produce BChl *c* derivatives, with additional methylation at 8^2-C and 12^1-C, dramatically improved the light harvesting properties of chlorosomes. The improved light harvesting of the suprastructures produced from BChl *c* provided the natural selection that led to the extension of the BChl *c*/*d*/*e* biosynthetic pathway.

■ ASSOCIATED CONTENT

⑤ Supporting Information

The ^{13}C and ^{1}H solution and solid-state chemical shifts of BChl *c* from the *bchQR* and WT chlorosomes as well as the aggregation shifts. This material is available free of charge via the Internet at http://pubs.acs.org.

■ AUTHOR INFORMATION

Corresponding Author

*Leiden Institute of Chemistry, Leiden University, P.O. Box 9502, 2300 RA Leiden, The Netherlands. E-mail: groot_h@lic.leidenuniv.nl. Telephone: +31 71 5274539.

Present Addresses

[⊥]R³, section Fundamental Aspects of Materials and Energy, Faculty of Applied Sciences, Delft University of Technology, Mekelweg 15, 2629 JB Delft, The Netherlands.

@Department of Bioscience and Biotechnology, Faculty of Science and Engineering, Ritsumeikan University, Kusatsu, Shiga 525-8577, Japan.

◼ ACKNOWLEDGMENTS

◼ ABBREVIATIONS

NMR, nuclear magnetic resonance; BChl, bacteriochlorophyll; [E,M], [8-ethyl,12-methyl]; [E,E], [8-ethyl,12-ethyl]; [Pr,E], [8-n-propyl,12-ethyl]; EM, electron microscopy; DFT, density functional theory; MAS, magic-angle-spinning; TMS, tetramethylsilane; BLYP, Becke−Lee−Yang−Parr; RFDR, radiofrequency-driven recoupling.

◼ REFERENCES

(1) Overmann, J., Cypionka, H., and Pfennig, N. (1992) An extremely low-light-adapted phototrophic sulfur bacterium from the Black Sea. *Limnol. Oceanogr. 37*, 150−155.

(2) Frigaard, N. U., and Bryant, D. A. (2006) Chlorosomes: Antenna organelles in photosynthetic green bacteria. In *Microbiology Monographs* (Shively, J. M., Ed.) pp 79−114, Springer-Verlag, Berlin.

(3) Frigaard, N. U., Li, H., Milks, K. J., and Bryant, D. A. (2004) Nine mutants of *Chlorobium tepidum* each unable to synthesize a different chlorosome protein still assemble functional chlorosomes. *J. Bacteriol. 186*, 646−653.

(4) Holzwarth, A. R., Griebenow, K., and Schaffner, K. (1990) A photosynthetic antenna system which contains a protein-free chromophore aggregate. *Z. Naturforsch., C: Biosci. 45*, 203−206.

(5) Ganapathy, S., Oostergetel, G. T., Wawrzyniak, P. K., Reus, M., Gomez Maqueo Chew, A., Buda, F., Boekema, E. J., Bryant, D. A., Holzwarth, A. R., and de Groot, H. J. M. (2009) Alternating *syn-anti* bacteriochlorophylls form concentric helical nanotubes in chlorosomes. *Proc. Natl. Acad. Sci. U.S.A. 106*, 8525−8530.

(6) Holzwarth, A. R., Müller, M. G., and Griebenow, K. (1990) Picosecond energy transfer kinetics between pigment pools in different preparations of chlorosomes from the green bacterium *Chloroflexus aurantiacus* ok-70-fl. *J. Photochem. Photobiol., B 5*, 457−465.

(7) Prokhorenko, V. I., Holzwarth, A. R., Müller, M. G., Schaffner, K., Miyatake, T., and Tamiaki, H. (2002) Energy transfer in supramolecular artificial antennae units of synthetic zinc chlorins and co-aggregated energy traps. A time-resolved fluorescence study. *J. Phys. Chem. B 106*, 5761−5768.

(8) Prokhorenko, V. I., Steensgaard, D. B., and Holzwarth, A. R. (2003) Exciton theory for supramolecular chlorosomal aggregates: 1. Aggregate size dependence of the linear spectra. *Biophys. J. 85*, 3173−3186.

(9) Kim, H., Li, H., Maresca, J. A., Bryant, D. A., and Savikhin, S. (2007) Triplet exciton formation as a novel photoprotection mechanism in chlorosomes of *Chlorobium tepidum*. *Biophys. J. 93*, 192−201.

(10) Tamiaki, H., Holzwarth, A. R., and Schaffner, K. (1992) A synthetic zinc chlorin aggregate as a model for the supramolecular antenna complexes in the chlorosomes of green bacteria. *J. Photochem. Photobiol., B 15*, 355−360.

(11) Huber, V., Lysetska, M., and Würthner, F. (2007) Self-assembled single- and double-stack π-aggregates of chlorophyll derivatives on highly ordered pyrolytic graphite. *Small 3*, 1007−1014.

(12) Schenning, A. P. H. J., and Meijer, E. W. (2005) Supramolecular electronics; nanowires from self-assembled π-conjugated systems. *Chem. Commun.,*, 3245−3258.

(13) Zietz, B., Prokhorenko, V. I., Holzwarth, A. R., and Gillbro, T. (2006) Comparative study of the energy transfer kinetics in artificial BChl e aggregates containing a BChl a acceptor and BChl e-containing chlorosomes of *Chlorobium phaeobacteroides*. *J. Phys. Chem. B 110*, 1388−1393.

(14) Oostergetel, G. T., Reus, M., Gomez Maqueo Chew, A., Bryant, D. A., Boekema, E., and Holzwarth, A. R. (2007) Long-range organization of bacteriochlorophyll in chlorosomes of *Chlorobium tepidum* investigated by cryo-electron microscopy. *FEBS Lett. 581*, 5435−5439.

(15) Gomez Maqueo Chew, A., Frigaard, N. U., and Bryant, D. A. (2007) Bacteriochlorophyllide c C-8[2] and C-12[1] methyltransferases are essential for adaptation to low light in *Chlorobaculum tepidum*. *J. Bacteriol. 189*, 6176−6184.

(16) Balaban, T. S., Holzwarth, A. R., Schaffner, K., Boender, G. J., and de Groot, H. J. M. (1995) CP-MAS ^{13}C-NMR dipolar correlation spectroscopy of ^{13}C-enriched chlorosomes and isolated bacteriochlorophyll-c aggregates of *Chlorobium tepidum*: The self-organization of pigments is the main structural feature of chlorosomes. *Biochemistry 34*, 15259−15266.

(17) van Rossum, B. J., Steensgaard, D. B., Mulder, F. M., Boender, G. J., Schaffner, K., Holzwarth, A. R., and de Groot, H. J. M. (2001) A refined model of the chlorosomal antennae of the green bacterium *Chlorobium tepidum* from proton chemical shift constraints obtained with high-field 2-D and 3-D MAS NMR dipolar correlation spectroscopy. *Biochemistry 40*, 1587−1595.

(18) Tian, Y., Camacho, R., Thomsson, D., Reus, M., Holzwarth, A. R., and Scheblykin, I. G. (2011) Organization of bacteriochlorophylls in individual chlorosomes from *Chlorobaculum tepidum* studied by 2-dimensional polarization fluorescence microscopy. *J. Am. Chem. Soc. 133*, 17192−17199.

(19) Wahlund, T. M., Woese, C. R., Castenholz, R. W., and Madigan, M. T. (1991) A thermophilic green sulfur bacterium from New Zealand hot springs, *Chlorobium tepidum* sp. nov. *Arch. Microbiol. 156*, 81−90.

(20) Steensgaard, D. B., Wackerbarth, H., Hildebrandt, P., and Holzwarth, A. R. (2000) Diastereoselective control of bacteriochlorophyll e aggregation. 3[1]-S-BChl e is essential for the formation of chlorosome-like aggregates. *J. Phys. Chem. B 104*, 10379−10386.

(21) Bennett, A. E., Rienstra, C. M., Auger, M., Lakshmi, K. V., and Griffin, R. G. (1995) Heteronuclear decoupling in rotating solids. *J. Chem. Phys. 103*, 6951−6958.

(22) Bennett, A. E., Ok, J. H., Griffin, R. G., and Vega, S. (1992) Chemical-shift correlation spectroscopy in rotating solids: Radio frequency-driven dipolar recoupling and longitudinal exchange. *J. Chem. Phys. 96*, 8624−8627.

(23) Mulder, F. M., Heinen, W., van Duin, M., Lugtenburg, J., and de Groot, H. J. M. (1998) Spin diffusion with ^{13}C selection and detection for the characterization of morphology in labeled polymer blends with MAS NMR. *J. Am. Chem. Soc. 120*, 12891−12894.

(24) Wilhelm, M., Feng, H., Tracht, U., and Spiess, H. W. (1998) 2D CP/MAS ^{13}C isotropic chemical shift correlation established by ^{1}H spin diffusion. *J. Magn. Reson. 134*, 255−260.

(25) van Rossum, B. J., Förster, H., and de Groot, H. J. M. (1997) High-field and high-speed CP-MAS ^{13}C NMR heteronuclear dipolar-correlation spectroscopy of solids with frequency-switched *Lee-Goldburg* homonuclear decoupling. *J. Magn. Reson. 124*, 516−519.

(26) Frisch, M. J., Trucks, G. W., Schlegel, H. B., Scuseria, G. E., Robb, M. A., Cheeseman, J. R., Montgomery, J. A., Jr., Vreven, T., Kudin, K. N., Burant, J. C., Millam, J. M., Iyengar, S. S., Tomasi, J., Barone, V., Mennucci, B., Cossi, M., Scalmani, G., Rega, N., Petersson, G. A., Nakatsuji, H., Hada, M., Ehara, M., Toyota, K., Fukuda, R., Hasegawa, J., Ishida, M., Nakajima, T., Honda, Y., Kitao, O., Nakai, H., Klene, M., Li, X., Knox, J. E., Hratchian, H. P., Cross, J. B., Adamo, C., Jaramillo, J., Gomperts, R., Stratmann, R. E., Yazyev, O., Austin, A. J., Cammi, R., Pomelli, C., Ochterski, J. W., Ayala, P. Y., Morokuma, K.,

Voth, G. A., Salvador, P., Dannenberg, J. J., Zakrzewski, V. G., Dapprich, S., Daniels, A. D., Strain, M. C., Farkas, O., Malick, D. K., Rabuck, A. D., Raghavachari, K., Foresman, J. B., Ortiz, J. V., Cui, Q., Baboul, A. G., Clifford, S., Cioslowski, J., Stefanov, B. B., Liu, G., Liashenko, A., Piskorz, P., Komaromi, I., Martin, R. L., Fox, D. J., Keith, T., Al-Laham, M. A., Peng, C. Y., Nanayakkara, A., Challacombe, M., Gill, P. M. W., Johnson, B., Chen, W., Wong, M. W., Gonzalez, C., and Pople, J. A. (2004) *Gaussian 03*, revision C.02, Gaussian, Inc., Wallingford, CT.

(27) Becke, A. D. (1986) Density functional calculations of molecular bond energies. *J. Chem. Phys. 84*, 4524−4529.

(28) Lee, C. T., Yang, W. T., and Parr, R. G. (1988) Development of the Colle-Salvetti correlation-energy formula into a functional of the electron-density. *Phys. Rev. B 37*, 785−789.

(29) Facelli, J. C. (1998) Density functional theory calculations of the structure and the ^{15}N and ^{13}C chemical shifts of methyl bacteriopheophorbide *a* and bacteriochlorophyll *a*. *J. Phys. Chem. B 102*, 2111−2116.

(30) Ditchfield, R. (1972) Molecular orbital theory of magnetic shielding and magnetic susceptibility. *J. Chem. Phys. 56*, 5688−5691.

(31) Ditchfield, R. (1974) Self-consistent perturbation-theory of diamagnetism. 1. Gauge-invariant LCAO method for NMR chemical-shifts. *Mol. Phys. 27*, 789−807.

(32) Wolinski, K., Hinton, J. F., and Pulay, P. (1990) Efficient implementation of the gauge-independent atomic orbital method for chemical-shift calculations. *J. Am. Chem. Soc. 112*, 8251−8260.

(33) Jentzen, W., Song, X. Z., and Shelnutt, J. A. (1997) Structural characterization of synthetic and protein-bound porphyrins in terms of the lowest-frequency normal coordinates of the macrocycle. *J. Phys. Chem. B 101*, 1684−1699.

(34) Shelnutt, J. A., Song, X. Z., Ma, J. G., Jia, S. L., Jentzen, W., and Medforth, C. J. (1998) Nonplanar porphyrins and their significance in proteins. *Chem. Soc. Rev. 27*, 31−41.

(35) Guex, N., and Peitsch, M. C. (1997) SWISS-MODEL and the Swiss-PdbViewer: An environment for comparative protein modeling. *Electrophoresis 18*, 2714−2723.

(36) Ludtke, S. J., Baldwin, P. R., and Chiu, W. (1999) EMAN: Semiautomated software for high-resolution single-particle reconstructions. *J. Struct. Biol. 128*, 82−97.

(37) Boender, G. J. (1996) PhD thesis. Leiden University.

(38) Abraham, R. J., and Rowan, A. E. (1991) Nuclear magnetic resonance spectroscopy of chlorophyll. In *Chlorophylls* (Scheer, H., Ed.) pp 797−834, CRC Press, Boca Raton, FL.

(39) Wang, Z. Y., Umetsu, M., Kobayashi, M., and Nozawa, T. (1999) ^{13}C- and ^{15}N-NMR studies on the intact bacteriochlorophyll *c* dimers in solutions. *J. Am. Chem. Soc. 121*, 9363−9369.

(40) Umetsu, M., Hollander, J. G., Matysik, J., Wang, Z. Y., Adschiri, T., Nozawa, T., and de Groot, H. J. M. (2004) Magic-angle spinning nuclear magnetic resonance under ultrahigh field reveals two forms of intermolecular interaction within CH_2Cl_2-treated (3^1R)-type bacterio-chlorophyll *c* solid aggregate. *J. Phys. Chem. B 108*, 2726−2734.

(41) de Boer, I., Bosman, L., Raap, J., Oschkinat, H., and de Groot, H. J. M. (2002) 2D ^{13}C-^{13}C MAS NMR correlation spectroscopy with mixing by true ^{1}H spin diffusion reveals long-range intermolecular distance restraints in ultra high magnetic field. *J. Magn. Reson. 157*, 286−291.

(42) Lange, A., Seidel, K., Verdier, L., Luca, S., and Baldus, M. (2003) Analysis of proton-proton transfer dynamics in rotating solids and their use for 3D structure determination. *J. Am. Chem. Soc. 125*, 12640−12648.

(43) Ganapathy, S., van Gammeren, A. J., Hulsbergen, F. B., and de Groot, H. J. M. (2007) Probing secondary, tertiary, and quaternary structure along with protein-cofactor interactions for a helical transmembrane protein complex through H-1 spin diffusion with MAS NMR spectroscopy. *J. Am. Chem. Soc. 129*, 1504−1505.

(44) Strohmeier, M., Orendt, A. M., Facelli, J. C., Solum, M. S., Pugmire, R. J., Parry, R. W., and Grant, D. M. (1997) Solid state ^{15}N and ^{13}C NMR study of several metal 5,10,15,20-tetraphenylporphyrin complexes. *J. Am. Chem. Soc. 119*, 7114−7120.

(45) Holzwarth, A. R., and Schaffner, K. (1994) On the structure of bacteriochlorophyll molecular aggregates in the chlorosomes of green bacteria: A molecular modeling study. *Photosynth. Res. 41*, 225−233.

(46) Kakitani, Y., Koyama, Y., Shimoikeda, Y., Nakai, T., Utsumi, H., Shimizu, T., and Nagae, H. (2009) Stacking of bacteriochlorophyll *c* macrocycles in chlorosome from *Chlorobium limicola* as revealed by intermolecular ^{13}C magnetic-dipole correlation, X-ray diffraction, and quadrupole coupling in ^{25}Mg NMR. *Biochemistry 48*, 74−86.

(47) Ganapathy, S., Sengupta, S., Wawrzyniak, P. K., Huber, V., Buda, F., Baumeister, U., Würthner, F., and de Groot, H. J. M. (2009) Zinc chlorins for artificial light-harvesting self-assemble into antiparallel stacks forming a microcrystalline solid-state material. *Proc. Natl. Acad. Sci. U.S.A. 106*, 11472−11477.

(48) Jochum, T., Reddy, C. M., Eichhofer, A., Buth, G., Szmytkowski, J., Kalt, H., Moss, D., and Balaban, T. S. (2008) The supramolecular organization of self-assembling chlorosomal bacteriochlorophyll *c*, *d*, or *e* mimics. *Proc. Natl. Acad. Sci. U.S.A. 105*, 12736−12741.

(49) Herbst, W., and Hunger, K. (1997) *Industrial organic pigments: Production, properties, applications*, Wiley-VCH, Weinheim, Germany.

(50) Ishii, T., Kimura, M., Yamamoto, T., Kirihata, M., and Uehara, K. (2000) The effects of epimerization at the 3^1-position of bacteriochlorophylls *c* on their aggregation in chlorosomes of green sulfur bacteria. Control of the ratio of 3^1 epimers by light intensity. *Photochem. Photobiol. 71*, 567−573.

(51) Saga, Y., Shibata, Y., Ltoh, S., and Tamiaki, H. (2007) Direct counting of submicrometer-sized photosynthetic apparatus dispersed in medium at cryogenic temperature by confocal laser fluorescence microscopy: Estimation of the number of bacteriochlorophyll *c* in single light-harvesting antenna complexes chlorosomes of green photosynthetic bacteria. *J. Phys. Chem. B 111*, 12605−12609.

(52) Balaban, T. S., Holzwarth, A. R., and Schaffner, K. (1995) Circular dichroism study on the diastereoselective self-assembly of bacteriochlorophyll c_S. *J. Mol. Struct. 349*, 183−186.

(53) Chiefari, J., Griebenow, K., Griebenow, N., Balaban, T. S., Holzwarth, A. R., and Schaffner, K. (1995) Models for the pigment organization in the chlorosomes of photosynthetic bacteria: Diastereoselective control of *in vitro* bacteriochlorophyll *c*(s) aggregation. *J. Phys. Chem. 99*, 1357−1365.

(54) Mizoguchi, T., Hara, K., Nagae, H., and Koyama, Y. (2000) Structural transformation among the aggregate forms of bacterio-chlorophyll *c* as determined by electronic-absorption and NMR spectroscopies: Dependence on the stereoisomeric configuration and on the bulkiness of the 8-C side chain. *Photochem. Photobiol. 71*, 596−609.

(55) Pandit, A., and de Groot, H. J. M. (2011) Solid-state NMR applied to photosynthetic light-harvesting complexes. *Photosynth. Res. 111*, 219−226.